Available online at www.sciencedirect.com
ScienceDirect
Combustion and Flame 149 (2007) 448–462
Combustion and Flame
www.elsevier.com/locate/combustflame

Effect of multistage combustion on NO_x emissions in methane–air flames

Alejandro M. Briones, Sibendu Som, Suresh Aggarwal *

Department of Mechanical and Industrial Engineering, University of Illinois at Chicago, Chicago, IL 60607, USA

Received 31 July 2006; received in revised form 22 December 2006; accepted 31 January 2007

Available online 20 April 2007

Abstract

Coflow and counterflow methane–air flames are simulated over a complete partially premixed regime in order to characterize the effects of dominant combustion modes (i.e., single-, two-, and three-stage combustion) on NO_x emissions. Simulations employ a comprehensive numerical model that uses detailed descriptions of transport and chemistry (GRI-2.11 mechanism) and includes radiation effects. It is demonstrated that a complete partially premixed regime, which extends from premixed flames to triple flames and then to double flames, can be simulated by suitably varying the equivalence ratios in the fuel-rich and fuel-lean streams, while maintaining the global equivalence ratio fixed. Both counterflow and coflow simulations show that NO_x emissions decrease significantly from the premixed to the triple flame regime, and then increase from the triple to the double flame regime. Therefore, triple flames not only extend the rich and the lean flammability limits, but also exhibit superior NO_x characteristics compared to the corresponding premixed flames and double flames, with thermal, prompt, NNH-intermediate, and N_2O-intermediate routes being the important contributors (in descending order) to NO_x formation. Coflow and counterflow flames exhibit qualitatively similar NO_x characteristics in the entire partially premixed regime and an optimum level of partial premixing that yields the lowest NO_x emission. The quantitative differences in NO_x emissions between the two configurations can be attributed to geometry-dependent effects. In particular, compared to counterflow flames, the coflow flames have significantly larger flame volume and therefore lower peak temperature and NO_x emission index in the triple flame regime.

Keywords: Multistage combustion; NO_x emissions; Methane; Partial premixing; Triple and double flames

1. Introduction

An effective way to reduce emissions from diesel engine and gas turbine combustors is to use staged combustion, which involves multiple reaction zones such as rich premixed, lean premixed, and nonpremixed reaction zones. Flames associated with staged combustion belong to an important class of flames termed partially premixed flames, which includes triple or tribrachial flames, double flames, edge flames, and even lifted nonpremixed jet flames, since they often contain a triple or double flame structure at the flame base. A triple flame consists of a diffusion flame embedded between fuel-lean and fuel-rich premixed flames. Fuel is completely consumed in the two premixed flames and the intermediate fuel species, such as CO and H_2, are transported to and consumed

* Corresponding author. Fax: +1 (312) 413 0441.
E-mail address: ska@uic.edu (S. Aggarwal).

0010-2180/$ – see front matter
doi:10.1016/j.combustflame.2007.01.007

in the nonpremixed flame. The excess oxidizer that survives through the lean premixed flame is also consumed in the nonpremixed flame, which is stabilized at the stoichiometric mixture fraction. The structure of a triple flame is different from that of a premixed flame due to the existence of lean premixed and nonpremixed reaction zones in the former. Similarly, the triple flame structure differs from a double flame structure due to the existence of a lean premixed reaction zone. These differences in flame structures cause significant differences in their stability and emission characteristics.

Phillips first investigated the propagation of triple flames in a methane–air mixing layer that mimicked the roofs of coal mine roadways [1]. Subsequently, there has been significant interest in the study of these flames [2–13] due to their fundamental and practical relevance, especially with regards to nonpremixed flame stabilization, turbulent combustion, fire safety, autoignition, and flame spread. While the previous studies have examined the detailed structure and stability of these flames, they have not examined the emission characteristics in detail. It is well known that NO_x emission in a flame is closely related to its detailed structure, especially the distribution of radical species such as O, OH, and CH. Since a partially premixed flame contains multiple reaction zones, and its structure is determined by the thermal and chemical interactions between these reaction zones, its NO_x characteristics are expected to be significantly different from those of premixed and nonpremixed flames. Moreover, depending upon the level of premixing in the fuel and air streams, a partially premixed flame may be a triple flame containing three reaction zones or a double flame containing two reaction zones. Again, the NO_x characteristics of a triple flame can be expected to be different from those of a double flame. Therefore, our objective is to characterize the flame structure and NO_x emissions in the entire partially premixed regime, extending from premixed flames to double flames, and then to triple flames. While the global equivalence ratio is kept fixed, a family of premixed, double, and triple flames are simulated in both coflow and counterflow configurations, and their structures and NO_x characteristics are analyzed. In addition, the relative contributions of the various submechanisms, i.e., thermal, prompt, NNH-intermediate, NO_2, and N_2O-intermediate routes, to total NO_x are characterized in the entire partially premixed regime. Methane is selected as the fuel, since it is the simplest model hydrocarbon fuel and thereby serves as a starting point for investigating higher hydrocarbon fuels. Moreover, the chemical pathways of methane combustion are relatively well understood.

The present study is relevant from both fundamental and practical considerations. First of all, partially premixed flames are important in many combustion applications. Second, lifted flames in laminar [14–17] and turbulent [18,19] jets have been extensively studied in order to gain a fundamental understanding of flame liftoff and stabilization phenomena. These investigations have observed that depending upon the liftoff height and other conditions, their base structure can vary from a nonpremixed flame (single flame) to a double flame and to a triple flame. Therefore, a fundamental investigation of NO_x characteristics in the various combustion regimes is important from this perspective.

The present study is also relevant to NO_x emissions in diesel engines, since combustion in these engines is generally characterized by a partially premixed flame containing two reaction zones [20]. Moreover, recent studies [21,22] have demonstrated that NO_x emissions in diesel engines can be markedly reduced using multiple fuel injections, i.e., by splitting the injection process into two or more separate but controlled injections. However, a fundamental understanding of the phenomena regarding the effects of fuel injection partitioning on NO_x is still lacking. For instance, a single fuel injection in a diesel engine generally leads to a partially premixed (two-stage) combustion mode in which the fuel burns in two reaction zones. This partially premixed combustion mode and thereby the emission characteristics will be significantly modified by switching from single to multiple fuel injections. Controlled two-stage fuel injection, in which the fuel injection was split into two separate injections with a specified time delay, would lead to the formation of a fuel lean zone in the region surrounding the nonpremixed flame. This in turn would form a lean premixed flame around the periphery of a nonpremixed flame. Consequently, a two-stage fuel injection would modify the dominant combustion mode from one containing two reaction zones to a structure that had three reaction zones. Previous experimental and numerical studies [23,24] have shown that the lean premixed zone interacts synergistically with the nonpremixed zone and modifies its structure. Moreover, two-stage fuel injection would significantly increase the level of partial premixing (i.e., decrease ϕ) in the rich premixed zone, and thus modify the structures of all three reaction zones as well as their NO_x characteristics [25,26]. Therefore, it is of fundamental interest to characterize the flame structure and NO_x emissions in the entire partially premixed regime from the diesel engine perspective as well.

Our literature review indicates that fundamental studies dealing with the effects of dominant combustion modes on NO_x emissions are lacking, although some researchers have examined the effects of partial premixing on NO_x emissions in flames [11,12,

26–28]. Gore and Zhan [27] performed an experimental investigation of NO_x emission in coflow CH_4/air PPFs and found an optimum level of partial premixing that yielded the lowest NO_x emission index. However, a numerical investigation of NO emission in coflow CH_4/air PPFs reported by Zhu et al. [12] observed that the NO emission index increases monotonically with the increasing fuel stream equivalence ratio, reaching its maximum value for the diffusion flame. Tanoff et al. [28] conducted a numerical–experimental study of counterflow CH_4/air PPFs and observed a drastic change in NO emission during transition from a nearly merged flame structure to a double flame structure, while Li and Williams [25] observed that NO_x emission first increases and then decreases as the fuel stream equivalence ratio is increased. Xue and Aggarwal [26] reported a numerical investigation of NO_x emission in n-C_7H_{16}/air counterflow PPFs and observed an optimum level of partial premixing that yields the lowest NO_x emission index. The above cited studies considered PPFs containing two reaction zones, namely a premixed zone and a nonpremixed zone. Guo et al. [11] simulated a counterflow CH_4/air triple flame and observed that a triple flame produces more NO_x than the corresponding premixed flame. However, these two flames were established at different global equivalence ratios. In summary, while previous studies have examined NO_x emissions in partially premixed flames, they have not followed a systematic approach to characterize NO_x emissions in the entire partially premixed regime while keeping the global equivalence ratio fixed. In addition, the relative contributions of various submechanisms, i.e., thermal, prompt, NNH-intermediate, NO_2, and N_2O-intermediate routes, to total NO_x have not been characterized under different levels of partial premixing that include premixed, double, and triple flames.

In the present investigation, we examine the detailed flame structure and NO_x emission characteristics by simulating both coflow and counterflow flames at various levels of partial premixing while keeping the global equivalence ratio (ϕ) fixed. For a given global ϕ and strain rate, a counterflow configuration allows one to establish flames in the entire partially premixed regime, ranging from premixed (twin) flames to triple flames and to double flames. A coflow jet configuration, on the other hand, closely emulates practical flames and allows one to examine geometry-dependent effects on NO_x emissions. For both the configurations, simulations employ a comprehensive numerical model that uses a detailed description of chemistry and transport, and includes radiation effects. The relative contributions of the thermal, prompt, and other NO_x submechanisms are also characterized in the entire partially premixed regime. It should be noted that while many combustion applications occur at high pressures, the present study considers atmospheric flames, since the focus is on a fundamental investigation of the NO_x characteristics in the various partially premixed regimes. Moreover, the detailed reaction mechanisms that are currently available for methane oxidation and NO_x formation have yet to be validated for high-pressure partially premixed flames.

Another important issue concerning the present study is the justification for considering laminar partially premixed flames, since most practical flames are turbulent. Laminar flames are more tractable for simulations using detailed chemistry and transport models and to characterize the contributions of various NO_x submechanisms under different partially premixed combustion regimes. The determination of the relative importance of different pathways for NO_x formation for turbulent flames is computationally impractical at present. Moreover, laminar flamelets are relevant in describing turbulent combustion at large Damköhler numbers. The present study is, therefore, expected to provide useful data to describe the NO_x characteristics of partially premixed flamelets under a wide range of partial premixing.

2. Computational model

Both counterflow and coflow methane–air flames were simulated. The methodology for the computation of counterflow flames using the OPPDIF [29] code and the CHEMKIN package [30] has been described in several previous studies [31] and therefore, will not be repeated here. Simulations of axisymmetric coflow flames, established for various sets of rich and lean equivalence ratios, were performed using a computational model developed by Katta and co-workers [32,33]. Table 1 lists all the flames simulated in the counterflow and coflow configurations. For both the counterflow and coflow flames, detailed algorithms were used to compute the relevant thermodynamic and transport properties. The effect of radiation was included through an optically thin radiation model [16]. The flame and NO_x chemistries for coflow flames were modeled using the GRI-2.11 mechanism [34], while for counterflow flames, both the GRI-2.11 and GRI-3.0 [35] mechanisms were employed.

There are two main reasons for using the above mechanisms for our investigation. First, our major objective is to qualitatively examine the effects of dominant combustion modes (i.e., single-, two-, and three-stage combustion) on NO_x emissions using counterflow and coflow methane–air flames over the entire partially premixed regime. Therefore, we do not focus

Table 1
List of simulated counterflow ($a_S = 100$ and 50 s^{-1}) and coflow flames characterized in terms of the global (ϕ), fuel-rich (ϕ_R), and fuel-lean (ϕ_L) equivalence ratios

Flame name	$\phi = 1.0$		Counterflow ($a_S = 100\ s^{-1}$)		Coflow and counterflow ($a_S = 50\ s^{-1}$)	
	ϕ_R	ϕ_L	V_R (cm/s)	V_L (cm/s)	V_R (cm/s)	V_L (cm/s)
A	1.00	1.00	63.5	63.5	31.8	31.8
A1	1.00	1.00	–	–	63.5	63.5
B	1.25	0.9	37.0	90.1	18.1	45.0
B1	1.10	0.96	42.7	84.4	–	–
B2	1.20	0.90	43.0	84.1	–	–
B3	1.40	0.84	37.5	89.7	–	–
C	1.50	0.8	37.8	89.5	18.9	44.8
D	1.75	0.7	38.6	88.9	19.3	44.4
E[a]	2.00	0.6	–	–	19.7	44.1
F	2.25	0.5	40.1	87.7	20.1	43.8
G	2.50	0.4	40.9	87.1	20.4	43.5
H	2.75	0.3	41.7	86.5	20.8	43.3
I	3.00	0.2	42.5	85.9	21.2	42.9
J	3.25	0.1	43.2	85.2	21.6	42.6
K	3.50	0.0	44.0	84.7	22.0	42.3

Note. The inflow velocities at the fuel-rich (V_R) and fuel-lean (V_L) boundaries are also indicated.
[a] These flames are computed only in the coflow configuration.

on issues pertaining to the accuracy of GRI-2.11 and GRI-3.0 mechanisms with regard to the flame structure and NO_x predictions. These issues have been addressed in previous studies [1–4]. Second, various experimental and numerical results reported in the literature have not provided convincing evidence for preferring one mechanism over the other. The global flame predictions, such as laminar flame speeds, using these two mechanisms have shown good agreement with the experimental data [36]. The flame structures predicted using these mechanisms for a variety of flames also exhibit relatively negligible differences with the corresponding measured structures for temperature and major species profiles [31,45]. With respect to radical species profiles, differences are more pronounced but still within an acceptable range [37]. The NO predictions using the two mechanisms also show generally good qualitative agreement with experimental data for a variety of premixed, nonpremixed, and partially premixed flames. However, the quantitative differences have been found to be significant, depending upon the flame investigated [25,38,39,45]. Clearly, further research is needed to refine these mechanisms for NO formation in hydrocarbon flames. However, the results of this investigation regarding the effects of dominant combustion modes on NO_x emissions are not expected to change qualitatively depending upon the reaction mechanism.

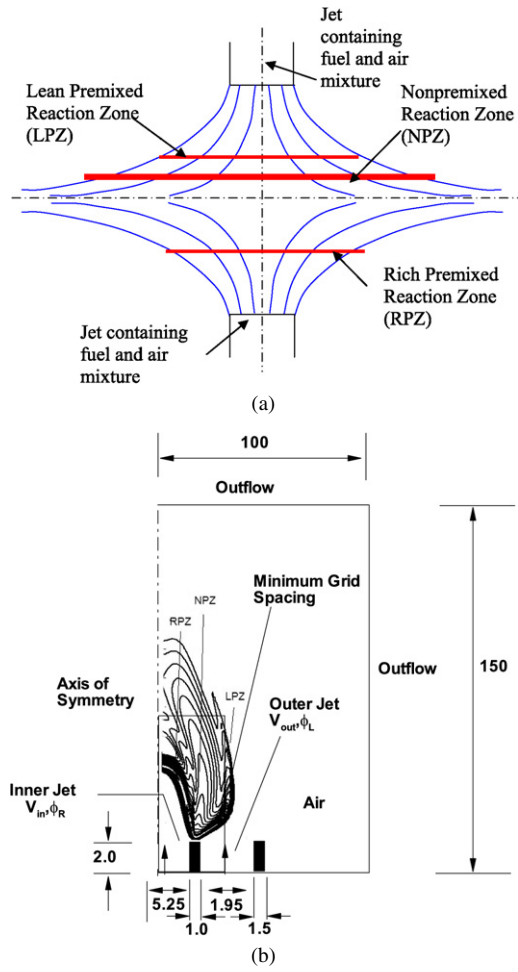

Fig. 1. A schematic of (a) counterflow flame configuration and (b) computational domain and boundary conditions used for the simulation of axisymmetric coflow flames.

A schematic of the methane–air triple flame in counterflow and coflow configurations is presented in Fig. 1. In a counterflow configuration, the various partially premixed flames including premixed, double, and triple flames are established by impinging fuel-rich and fuel-lean mixtures from two opposing nozzles. A premixed flame in this configuration contains two identical (twin) premixed reactions zones located on the opposite sides of the stagnation plane. A double flame, on the other hand, contains a rich premixed zone (RPZ) on the fuel-rich side and a nonpremixed zone (NPZ) on the oxidizer (fuel-lean) side, while a triple flame contains a RPZ on the fuel-rich side and a NPZ and a lean premixed zone (LPZ) on the fuel-lean side. Similarly, the various partially premixed flames are established in a coflow configuration by issuing fuel-rich and fuel-lean mixtures from two concentric tubes. For example, a coflow triple flame contains a

RPZ on the fuel-rich side, a LPZ on the fuel-lean side, and a NPZ located between the two premixed zones along the stoichiometric mixture fraction line.

For counterflow flame simulations, grid independence was achieved by controlling the values of the GRAD and CURV parameters and using adaptive regriding to resolve the structures of the various reaction zones for different partially premixed combustion modes. For coflow flames, a staggered, nonuniform grid system was used in order to resolve the steep gradients in the various reaction zones. The grid independence was established by decreasing the mesh size until a nearly grid-independent solution was obtained. The computational domain for coflow flames (cf. Fig. 1b) consisted of 150 × 100 mm in the axial (z) and radial (r) directions, respectively, and employed a nonuniform 401 × 115 grid. The minimum grid spacing required to capture the detailed flame structure associated with the premixed portions of the flame, especially the CH layer for accurately computing the prompt NO_x profile, was determined to be 0.1 mm. This minimum grid spacing is clustered in a rectangular region that extends from the centerline to 7.25 mm in the radial direction and from the inlet boundary to 32 mm in the axial direction. It is important to note that the flame thickness can vary significantly depending upon the level of partial premixing, with the smallest thickness corresponding to a stoichiometric premixed flame. For a typical coflow flame, such as Flame C (cf. Table 1), the CH layer thickness is about 1.2 mm and it contains about 10 grid points. The corresponding counterflow partially premixed flame in our simulation has a CH layer thickness of 1.5 mm. The worst case scenario in our study, in terms of resolving the CH layer, corresponds to the premixed flame (Flame A1) that has a CH layer thickness of 0.6 mm and contains 6 grid points, which is consistent with the measured CH layer thickness of 0.6 mm for a $\phi = 1.2$ premixed flame reported by Evertsen et al. [37]. Consequently, the radical layers are sufficiently resolved in our simulations. We have also addressed the grid resolution issue in our previous study [40].

Atmospheric, multistage methane–air flames were established using an annular concentric burner that consisted of a central tube with inner and outer diameters of 10.5 and 12.5 mm, respectively, which was surrounded by an outer concentric tube with inner and outer diameters of 16.4 and 19.4 mm, respectively. Fuel-rich and fuel-lean mixtures were introduced from the inner and outer tubes, respectively. The velocity profiles in both the tubes were assumed to be uniform. The fuel- and air-stream temperatures were fixed at 300 K. Special care was exercised in using identical conditions in the counterflow and coflow configurations, which included matching the mass flow rates and the cross-sectional areas of the fuel-rich and fuel-lean nozzles in the two configurations.

Since the various partially premixed regimes were simulated at a fixed global ϕ, a novel feature pertains to the specification of mixture composition in the two streams. A general procedure for both the counterflow and coflow flames is that for a given value of global ϕ, a premixed flame is first established using identical equivalence ratios in the fuel-rich and fuel-lean (oxidizer) streams, i.e., $\phi_R = \phi_L = \phi$. For the counterflow configuration, this corresponds to two identical or twin flames. Subsequently, ϕ_R is gradually increased while ϕ_L is correspondingly decreased so that the global ϕ is kept constant at a specified value, which was taken as unity in the present study. This leads to a transition from a premixed flame to a triple flame structure, containing three reaction zones. With further increase in ϕ_R and corresponding decrease in ϕ_L, the triple flame structure transitions to a double flame structure, as the lean premixed zone extinguishes when ϕ_L drops below a critical value. A list of counterflow and simulated flames at various values of ϕ_R and ϕ_L but at a constant global $\phi = 1.0$ is provided in Table 1.

Using the mass flow rates in the two streams, the global ϕ can be written as

$$\phi = \frac{\rho_{\mathrm{mix,R}} V_R Y_{\mathrm{F,R}} + \rho_{\mathrm{mix,L}} V_L Y_{\mathrm{F,L}}}{\nu(\rho_{\mathrm{mix,R}} V_R Y_{\mathrm{Ox,R}} + \rho_{\mathrm{mix,L}} V_L Y_{\mathrm{Ox,L}})}. \tag{1}$$

Here ρ_{mix}, V, and Y denote the mixture density, inflow velocity, and mass fraction, respectively. The subscripts F and Ox denote the fuel and oxidizer, respectively, and R and L denote the conditions in the rich and lean fuel streams, respectively. Since air is considered as the oxidizer, ν represents the stoichiometric fuel–air ratio. By using the expressions $Y_{\mathrm{F,R}} + Y_{\mathrm{Ox,R}} = 1$, $Y_{\mathrm{F,L}} + Y_{\mathrm{Ox,L}} = 1$, $\phi_R = Y_{\mathrm{F,R}}/(\nu Y_{\mathrm{Ox,R}})$, and $\phi_L = Y_{\mathrm{F,L}}/(\nu Y_{\mathrm{Ox,L}})$, Eq. (1) can be simplified as

$$\left(\frac{\phi_R - \phi}{\phi - \phi_L}\right) = \left(\frac{\rho_{\mathrm{mix,L}}}{\rho_{\mathrm{mix,R}}}\right)\left(\frac{V_L}{V_R}\right)\left(\frac{1 - Y_{\mathrm{F,L}}}{1 - Y_{\mathrm{F,R}}}\right). \tag{2}$$

For counterflow flames, the global strain rate (a_S) can be expressed as

$$a_S = \left(2|V_L|/l\right)\left\{1 + |V_R|\sqrt{\rho_{\mathrm{mix,R}}}/|V_L|\sqrt{\rho_{\mathrm{mix,L}}}\right\}. \tag{3}$$

Here l denotes the separation distance between the two nozzles. Once the rich (ϕ_R) and lean (ϕ_L) equivalence ratio values are assigned, the rich and lean inflow velocities are obtained by simultaneously solving Eqs. (2) and (3). It should be noted that although the inlet velocities and fuel–air compositions in the rich and lean streams change from one case to the other, the total fuel and oxidizer mass flow rates do not change for a given global ϕ and strain rate. For instance, the fuel and oxidizer mass fluxes are 0.08

and 1.37 kg/m^2/s, respectively, for all the counterflow flames established at $a_S = 100$ s^{-1}, and 0.04 and 0.685 kg/m^2/s, respectively, for flames established at $a_S = 50$ s^{-1}.

3. Results and discussion

3.1. Validation of the numerical models

The algorithms used for the simulation of coflow and counterflow flames have been extensively validated in previous studies. The algorithm for coflow flames has been validated using experimental data for burner-stabilized [33,41] and lifted partially premixed flames [23,42]. The validation has included the comparison of the predicted and measured flame topology and liftoff heights, as well as the temperature, velocity, and concentration fields. Similarly, the counterflow flame simulations using CHEMKIN software have been validated previously using experimental data for nonpremixed [43] and partially premixed methane–air flames [25,44–47] established under different conditions.

3.2. Counterflow multistage flame structure

Counterflow and coflow flames were simulated for a global equivalence ratio of $\phi = 1.0$. As indicated in Table 1, for a given global equivalence ratio (ϕ), ϕ_R and ϕ_L were varied in a systematic manner in order to establish flames over a wide partially premixed regime, which includes premixed flames, triple flames, and double flames. Fig. 2 presents the structure of several such flames established in the counterflow configuration at a stain rate of $a_S = 100$ s^{-1}. The flame structure is depicted in terms of the heat release rate profiles plotted with respect to the stagnation plane. The fuel-rich mixture enters the computational domain from the left side, whereas the lean mixture enters from the right side. Flame A represents a typical twin flame, established with $\phi_R = \phi_L$, containing two identical premixed reaction zones identified by the two heat release rate peaks.

As ϕ_R is increased, with a corresponding decrease in ϕ_L, the premixed flame transitions to a triple flame (Flame C) containing three reaction zones, as a nonpremixed reaction zone (NPZ) is formed in between the rich premixed (RPZ) and lean premixed (LPZ) zones. The three reaction zones are clearly indicated by the heat release rate profiles. The NPZ is formed as the reactants CH_4 and O_2 are consumed in the RPZ, producing "intermediate" fuel species CO and H_2, which are transported to and consumed in the NPZ. In contrast, while CH_4 is completely consumed in the LPZ, O_2 is only partially consumed, with the remaining O_2 transported to the NPZ, where it reacts with the "intermediate" fuel species. With further increase in ϕ_R and corresponding decrease in ϕ_L, both the rich and lean premixed reaction zones move toward the stagnation plane, i.e., downstream from the respective nozzles, as indicated by the heat release rate peaks for Flames C, E, and H, since the laminar burning velocities associated with the RPZ and LPZ decrease. As a consequence, the interactions between the three reaction zones are enhanced due to the reduced separation distances between them and the flame volume decreases. In addition, the heat release rate peaks corresponding to RPZ and LPZ decrease, while that corresponding to NPZ increases. It is important to note that the locations of the rich and lean premixed reaction zones are determined by a balance between the stretched laminar burning velocity and the local flow velocity. With further increase in ϕ_R and a corresponding decrease in ϕ_L, both the RPZ and LPZ become weaker, and as ϕ_L decreases below a certain critical value, the LPZ is extinguished and the triple flame structure transitions to a double flame structure, as illustrated by Flame K. Therefore, the computed heat release rate profiles in Fig. 2 clearly indicate that by suitably varying ϕ_R and ϕ_L, while maintaining the global ϕ fixed, it is possible to simulate the entire partially premixed regime.

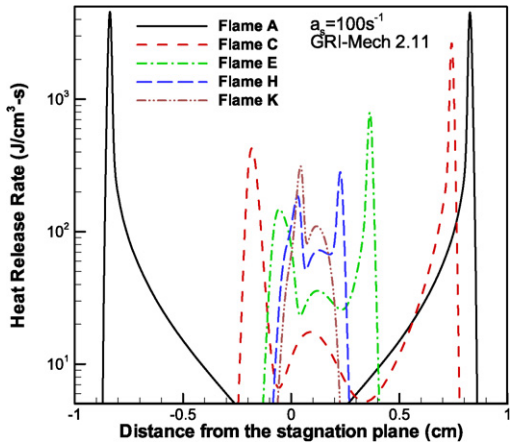

Fig. 2. Predicted heat release rate plotted as a function of distance from the stagnation plane for various multistage counterflow methane–air flames established at $\phi_R = \phi_L = 1.0$ (Flame A), $\phi_R = 1.5$ and $\phi_L = 0.8$ (Flame C), $\phi_R = 2.0$ and $\phi_L = 0.6$ (Flame E), $\phi_R = 2.75$ and $\phi_L = 0.3$ (Flame H), and $\phi_R = 3.5$ and $\phi_L = 0.0$ (Flame K). The global equivalence ratio is $\phi = 1.0$ and the global strain rate is $a_S = 100$ s^{-1}.

Since these multistage flames contain a premixed reaction zone, it is of interest to compute their stretched and the corresponding unstretched flame speeds. Fig. 3 presents the predicted stretched flame speeds (extracted from the computed results), as well

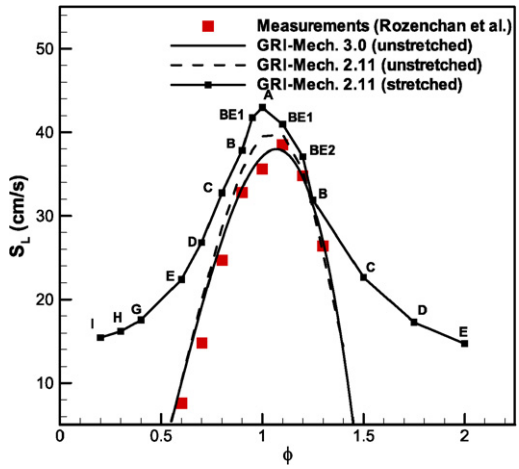

Fig. 3. Measured and predicted laminar flame speeds as a function of equivalence ratio. The predicted stretched flame speed corresponds to the flame speed extracted from the computed multistage flames shown in Fig. 2. The letters indicate the flame name from which each stretched flame speed was extracted. The measured flame speeds are taken from Rozenchan et al. [36].

as the measured [36] and predicted unstretched flame speeds, as a function of equivalence ratio. The predicted unstretched flame speeds are shown for both the GRI-2.11 and GRI-3.0 mechanisms. While both the mechanisms are able to reproduce the measured flame speeds, the GRI-2.11 mechanism slightly overpredicts the flame speeds near the stoichiometric conditions. The stretched flame speeds are generally larger than the corresponding unstretched flame speeds. There are two plausible explanations for this: (i) diffusive–thermal instability, and (ii) interactions between the nonpremixed and premixed reaction zones. For methane–air flames the Lewis number is Le < 1 for $\phi < 1$, and shifts to Le > 1 for $\phi > 1$ [48]. Therefore, when the lean methane–air flame is positively stretched the flame speed increases, and when the rich methane–air flame is positively stretched the flame speed decreases. Notice that the stretched flame speed increases substantially above the unstretched flame speed even for $\phi_L = 0.9$ (Flame B), for which there is no significant interaction between the premixed and nonpremixed reaction zones (cf. Fig. 2). This suggests that the increase in stretched flame speed in lean near-stoichiometric flames (i.e., Flames B1, B, and C) and stoichiometric premixed flames (i.e., Flame A) is due to diffusive–thermal instability. Under leaner conditions, the increase in flame speed is also due to thermal interaction between the nonpremixed and lean premixed reaction zones. On the other hand, the increase in the stretched flame speed under fuel-rich conditions is due to the interaction between the nonpremixed and rich premixed reaction zones, as diffusive–thermal instability would rather decrease the flame speed. The overall effect of diffusive–thermal instability and interactions between the reaction zones is to increase both the lean and rich flammability limits, as indicated by the increased flame speed and the wider laminar burning velocity profile compared to that corresponding to the freely propagating flames. Therefore, as indicated in Fig. 3, a triple flame can extend both the rich and the lean flammability limits. For example, a lean premixed zone is established with ϕ_L as low as 0.2 (Flame I), whereas the typical flammability limit is 0.46 [49]. Similarly, a rich premixed zone is established with ϕ_R as high as 2.0 (Flame E), whereas the typical flammability limit is 1.4.

3.3. NO_x characteristics of counterflow multistage flames

Having illustrated that methane–air flames can be established for a wide partially premixed regime, we now examine their NO_x emission characteristics. Fig. 4a presents the peak flame temperature and mole fractions of NO, O, and CH, while Fig. 4b presents the total NO emission index (EINO) plotted as a function of ϕ_R and ϕ_L for various PPFs established at a global $\phi = 1.0$ and $a_S = 100\ s^{-1}$. The O and CH radicals are considered as the primary precursors for thermal and prompt NO, respectively. EINO represents the ratio of total NO production rate to total fuel consumption rate and has been extensively used in the literature to quantify and compare the global NO emission characteristics of different flames. EINO is defined as [50,51]

$$\mathrm{EINO} = \frac{1000 \int_0^L \mathrm{MW}_{\mathrm{NO}} \omega_{\mathrm{NO}}\, \mathrm{d}x}{-\int_0^L \mathrm{MW}_{\mathrm{CH_4}} \omega_{\mathrm{CH_4}}\, \mathrm{d}x}\ (\mathrm{g\ NO/kg\ CH_4}). \tag{4}$$

Here ω is the production/consumption rate, MW the molecular weight, and L the separation distance between the two nozzles. The total CH_4 consumption and NO production rates are plotted in Fig. 4c. The NO emission indices of the thermal, prompt, N_2O-intermediate, and NNH-intermediate mechanisms, as well as their sum (thermal + prompt + N_2O + NNH), are also plotted in Fig. 4b. Computing the individual contribution of each submechanism to total NO_x required five simulations for each simulated flame. The first simulation was performed using the complete NO_x mechanism, while each of the other four simulations was performed using one of the submechanisms at a time. For example, the contribution of thermal NO was computed by suppressing all the reactions associated with the prompt, NNH-intermediate, and N_2O-intermediate routes. It is also important to mention in this context that for all the partially premixed

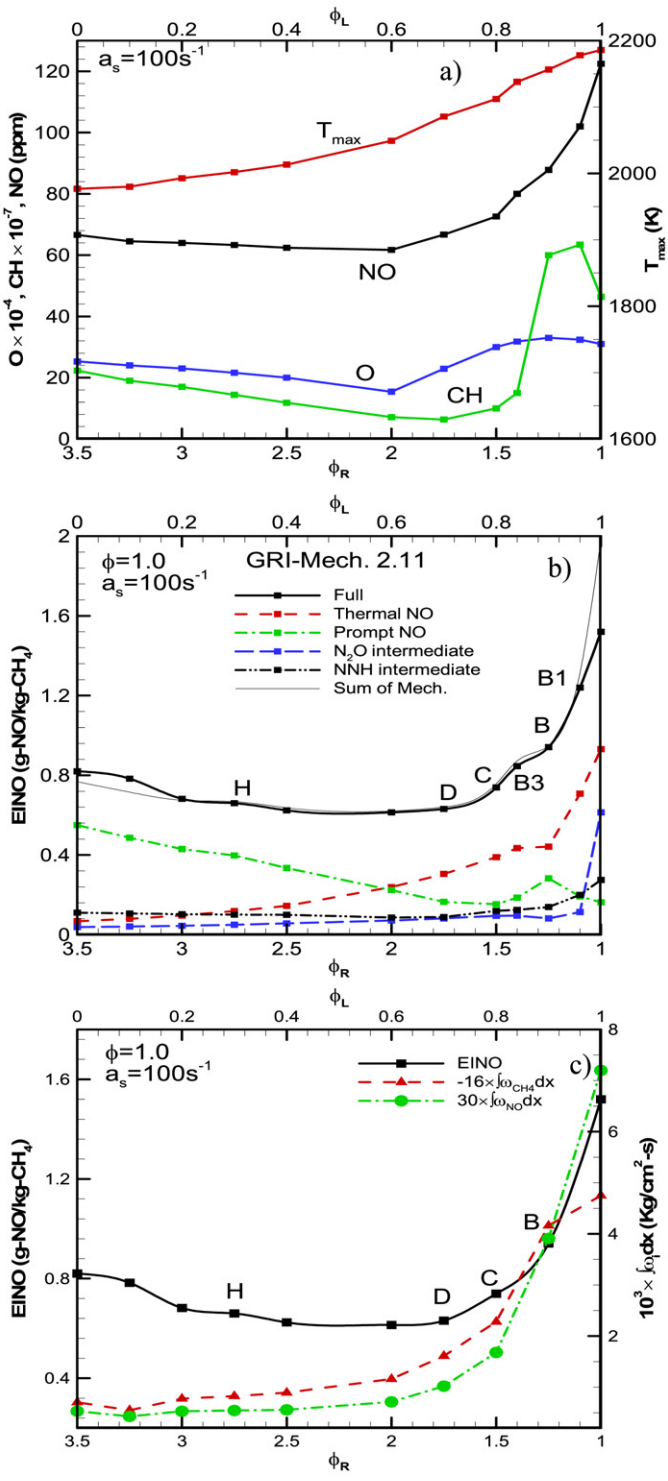

Fig. 4. Maximum flame temperature (T_{max}) and mole fractions of NO, CH, and O species (a). NO emission index (EINO) as a function of ϕ_R and ϕ_L for a global $\phi = 1.0$ and strain rate $a_S = 100\ s^{-1}$ are also shown (b). The NO emission indices for the thermal, prompt, N_2O-intermediate, and NNH-intermediate mechanisms, as well as the sum (thermal + prompt + N_2O + NNH) of the individual contributions to EINO, are also presented. The overall NO production (ω_{NO}) and CH_4 consumption ($-\omega_{CH_4}$) rate are presented (c). Note that for each ϕ_R there is a corresponding ϕ_L.

flames simulated in the present study, the contribution of NO_2 to total NO_x was found to be negligible. This is consistent with previous results concerning NO_x emission in nonpremixed and partially premixed flames [12,26,27,51].

The twin premixed flame (Flame A) is characterized by the highest temperature peaks, as the fuel oxidation occurs under stoichiometric conditions, and consequently, the total EINO is maximum (cf. Fig. 4b). With increase in ϕ_R and corresponding decrease in ϕ_L, there is a transition from a premixed (twin) flame regime to a triple flame regime (from right to left in Fig. 3), i.e., from Flame A to Flame B, and the total EINO, peak flame temperature, and thermal EINO decrease, whereas the prompt EINO increases. The decrease in thermal EINO is due to the decrease in peak flame temperature and O mole fraction (cf. Fig. 4a), while the increase in prompt EINO is due to the increase in CH mole fraction, as a larger amount of CH is produced in the rich premixed zone. There is also a local CH peak at $\phi_R \approx 1.2$, indicating that the maximum in CH and prompt NO mole fractions occurs under slightly fuel-rich conditions rather than under stoichiometric conditions.

As ϕ_R is increased from 1.25 to 1.5 with a corresponding decrease in ϕ_L from 0.9 to 0.8 (i.e., from Flame B to Flame C), both the thermal EINO and prompt EINO decrease, and, consequently, the total EINO also decreases. The decrease in prompt EINO is due to the significant decrease in CH mole fraction, whereas the decrease in thermal NO is due to reduction in flame temperature and O mole fraction. Further increasing ϕ_R and decreasing ϕ_L causes a reversal in the above trend; i.e., the total EINO now increases. This can be attributed to the fact that the prompt EINO becomes the major contributor to NO, and since the prompt EINO now increases, the total EINO also increases. A closer examination of NO production rate and fuel consumption rate indicated that for ϕ_R between 1.0 and 1.5 (i.e., from Flame A to Flame C), the NO production rate decreases faster than the fuel consumption rate (cf. Fig. 4c), and, consequently, the EINO decreases in this range. However, as ϕ_R exceeds 1.5, the trend reverses; i.e., the fuel consumption rate decreases at a faster rate than the NO production rate. Consequently, the EINO increases going from Flame D to Flame K (double flame regime).

An important observation from the above results pertains to the existence of a partially premixed (triple flame) regime for which both the peak NO mole fraction and the NO emission index have the lowest values compared to those for the corresponding premixed and partially premixed (double) flames established at the same global ϕ. This suggests that switching from a single-stage or a two-stage combustion mode to a three-stage combustion mode could lead to lower NO emissions in diesel engines and gas turbines. There are two other noteworthy observations from Fig. 4b. First, the emission indices (EINO) of NNH and N_2O-intermediate mechanisms are generally small compared to those of thermal and prompt mechanisms and decrease as the flames transition from the premixed regime (Flame A) to the triple flame regime (Flames B, C, D, E), and then to the double flame regime (Flames G, H, J, I K). Second, there is some difference between the total EINO computed using the full NO chemistry and the sum of EINO computed from each of the four individual contributions, implying some interactions between the individual NO formation pathways. However, this difference is small and does not have any effect on the important conclusion regarding the existence of an optimum level of partial premixing in the triple flame regime, which yields the lowest NO emissions.

3.4. *Effect of strain rate on NO emission in counterflow multistage flames*

Since most practical flames are turbulent, involving a wide range of strain rates, it is of interest to examine the effect of strain rate on NO_x emission in multistage laminar flames. Fig. 5 presents the peak flame temperature and NO mole fraction plotted versus ϕ_R and ϕ_L for various PPFs established at a global $\phi = 1.0$ and strain rates of $a_S = 100$ and 50 s^{-1}. Consistent with the extensive data reported in the literature [52] concerning the effect of strain rate on NO formation, our results indicate that decreasing the strain rate increases the flame temperature and, thereby, the NO mole fraction for the entire partially premixed regime investigated, since the residence time is increased. However, the qualitative behavior regarding the effect of partial premixing on NO_x emission and the existence of an optimum level of partial premixing remains the same for the two strain rates. We also computed the NO emission indices of the total, thermal, prompt, N_2O-intermediate, and NNH-intermediate mechanisms for various PPFs (similar to Fig. 4) established at a global strain rate of $a_S = 50\ s^{-1}$. These results (not shown here) were similar to those presented in Fig. 4. Therefore, it is reasonable to expect that conclusions regarding the existence of an optimum level of partial premixing (in the triple flame regime) will hold at all strain rates far from extinction, although we have presented results for only two global strain rates.

3.5. *Coflow multistage flame structure*

In the preceding section, we demonstrated that at a fixed global ϕ, a complete partially premixed

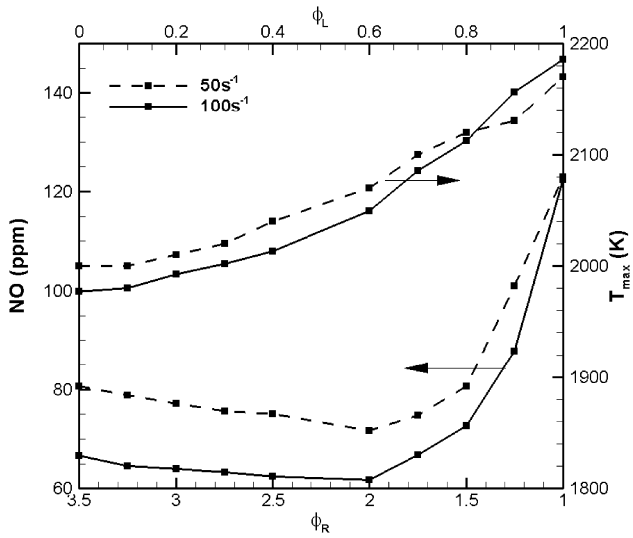

Fig. 5. Maximum flame temperature (T_{max}) and mole fractions of NO as a function of ϕ_R and ϕ_L for a global $\phi = 1.0$ and strain rates $a_S = 100$ and 50 s^{-1}.

regime could be simulated in a counterflow configuration by suitably varying the rich and lean equivalence ratios. Since a coflow jet configuration more closely emulates practical flames, it is of interest to extend the preceding analysis to this configuration. Fig. 6 presents the images of several partially premixed flames, in terms of heat release rate contours, established in the coflow configuration with inflow velocities corresponding to those for the counterflow flames with a strain rate of $a_S = 50\ s^{-1}$. These images demonstrate that at a fixed global ϕ, the entire partially premixed regime can also be simulated in a coflow configuration by suitably specifying the rich (ϕ_R) and lean (ϕ_L) equivalence ratios. Similarly to counterflow flames, as ϕ_R is increased, with corresponding decrease in ϕ_L, the coflow flames transition from premixed flames[1] to triple flames and then to double flames. The heat release rate contours also indicate that the flame length increases during this transition, since as ϕ_R is increased (i.e., the level of partial premixing is reduced), it increases the chemical time and, consequently, the length of the rich premixed zone. An increase in flame length implies that the flame volume increases going from Flame A to Flame K. This represents a major difference between the counterflow and coflow flames, since the flame volume decreases from Flame A to Flame K in the counterflow configuration. This difference leads to a lower NO_x emission index for coflow flames than for counterflow flames, as discussed in the next section. It is also important to mention that all the coflow flames simulated in the present study exhibited well-organized oscillations induced by buoyant acceleration, so care was taken in comparing these flames at the same phase angle.

Another important observation from Fig. 6 is that Flames D through K correspond to typical partially premixed flames, with either a triple flame structure (Flames D through I) or a double flame structure (Flames J and K), and are stabilized at the burner rim (inner insert). However, Flames A and B seem to flash back into the burner, which suggests that the inflow velocities are lower than the laminar burning velocities for these flames. In order to confirm this observation, we recomputed Flames A and B by doubling the inflow flow velocities and observed no flashback for the latter case. Fig. 7 presents the temperature and heat release rate contours for Flame A and Flame A1, corresponding to inflow velocities of 31.5 and 63.0 cm/s, respectively. These contours clearly indicate that by increasing the inflow velocity, the flashback is avoided, and the two premixed reaction zones of Flame A1 are stabilized at the burner rim.

3.6. NO_x characteristics of coflow multistage flames

Having examined the structure of coflow flames, we now examine their NO_x characteristics. As mentioned in the preceding section, since Flames A ($\phi_R = \phi_L = 1.0$) and B ($\phi_R = 1.25$ and $\phi_L = 0.9$) flash back into the burner, we recomputed these two flames (termed as Flames A1 and B1) by doubling the inflow velocity and observed no flashback. Consequently, we used the results of Flames A1 and B1, rather than

[1] Simulations indicate flashback for coflow Flames A and B. This issue is discussed later in this section.

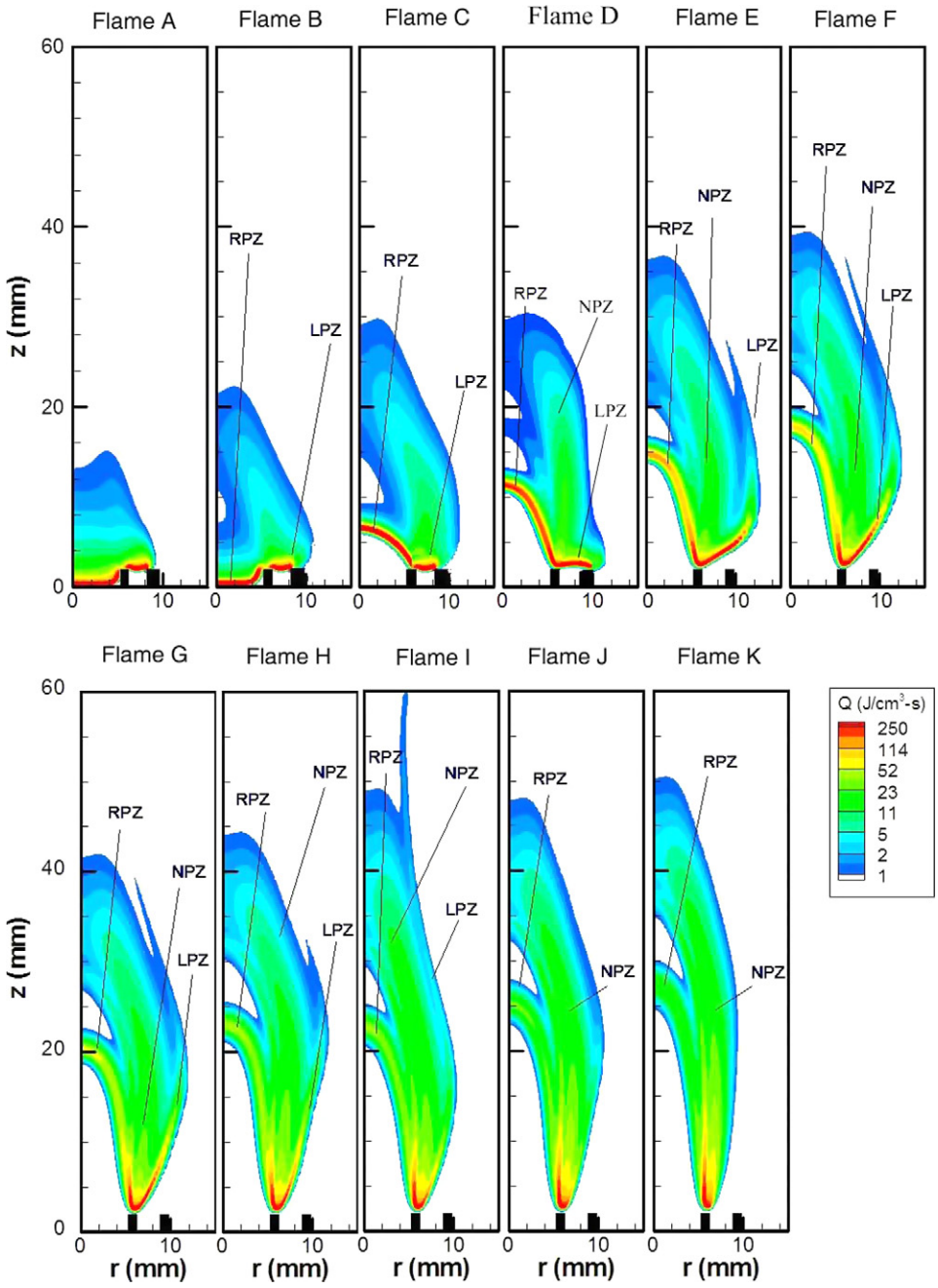

Fig. 6. Structures of coflow flames shown in terms of the heat release rate contours (Q) for different ϕ_R and ϕ_L cases, but all at a fixed ϕ. The multiple reaction zones are also indicated, with RPZ, LPZ, and NPZ representing, respectively, the rich, lean, and nonpremixed reaction zones.

those of Flames A and B, in characterizing the effects of partial premixing on NO_x emissions. Fig. 8 presents the instantaneous structures of Flames A1 ($\phi_R = \phi_L = 1.0$), C ($\phi_R = 1.5$ and $\phi_L = 0.8$), and K ($\phi_R = 3.5$ and $\phi_L = 0.0$) in terms of temperature contours, velocity vectors, and NO mole fraction contours. These three flames are representatives of the premixed flame regime (Flame A1), the triple flame regime (Flame C), and the double flame regime (Flame K), respectively. As indicated by the temperature and NO contours, most of the NO is formed in the high-temperature region (i.e., $T \geqslant 1800$ K) lo-

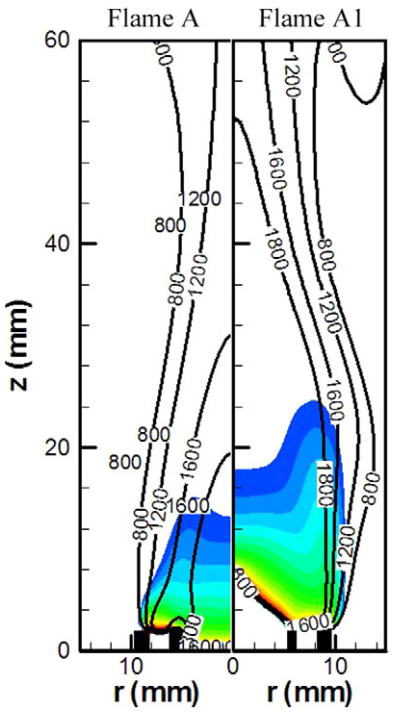

Fig. 7. Structures of coflow premixed Flames A and A1 in terms of heat release rate (rainbow scheme) and temperature (lines) contours. The temperature values are indicated in the labels with the units in Kelvin.

cated downstream of the burner rim and characterized by relatively low heat release rates and moderate velocities. The premixed flame (A1) contains a relatively larger high-temperature region and thereby produces the largest amount of NO compared to the triple (Flame C) and double (Flame K) partially premixed flames. On the other hand, Flame C produces the smallest amount of NO compared to Flames A1 and K, since the peak temperatures are lower in this flame, implying a significant reduction in thermal NO. Therefore, similarly to counterflow flames, coflow flames also exhibit an optimum level of partial premixing that yields the lowest NO emissions. The optimum values of ϕ_R and ϕ_L for a fixed global $\phi = 1.0$ are quantified in Fig. 10.

As mentioned earlier, the coflow flames simulated in the present study exhibit well-organized oscillations induced by buoyant acceleration. These oscillations cause fluctuations in NO concentrations and emissions as indicated in Fig. 9, which presents the temporal evolution of maximum NO mole fraction and EINO for several coflow flames. The EINO for coflow flames is defined as

$$\mathrm{EINO} = \frac{1000 \int_0^{Lz} \int_0^{Lr} \mathrm{MW_{NO}} \omega_{\mathrm{NO}} r \,\mathrm{d}r \,\mathrm{d}z}{-\int_0^{Lz} \int_0^{Lr} \mathrm{MW_{CH_4}} \omega_{\mathrm{CH_4}} r \,\mathrm{d}r \,\mathrm{d}z} \quad (\mathrm{g\ NO/kg\ CH_4}), \tag{5}$$

where Lr and Lz are the radial and axial lengths of the computational domain, respectively.

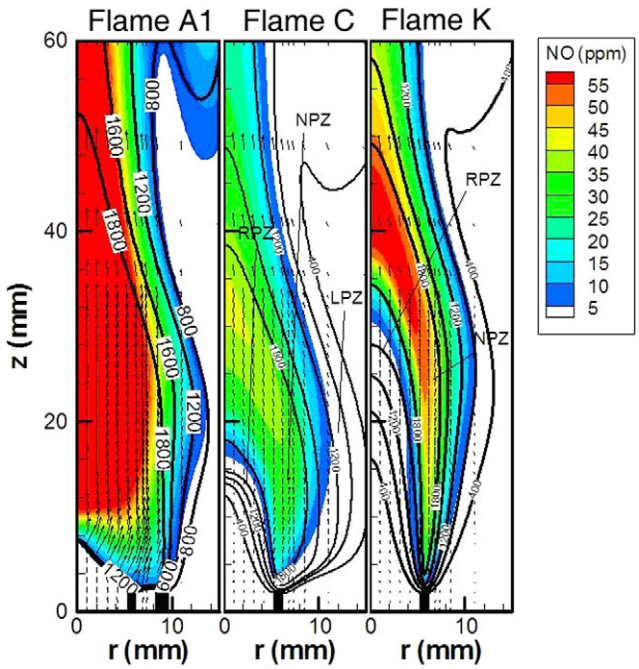

Fig. 8. Temperature contours, NO mole fraction contours, and velocity vectors for Flame A1 ($\phi_R = \phi_L = 1.0$), Flame C ($\phi_R = 1.5$ and $\phi_L = 0.8$), and Flame K ($\phi_R = 3.5$ and $\phi_L = 0.0$).

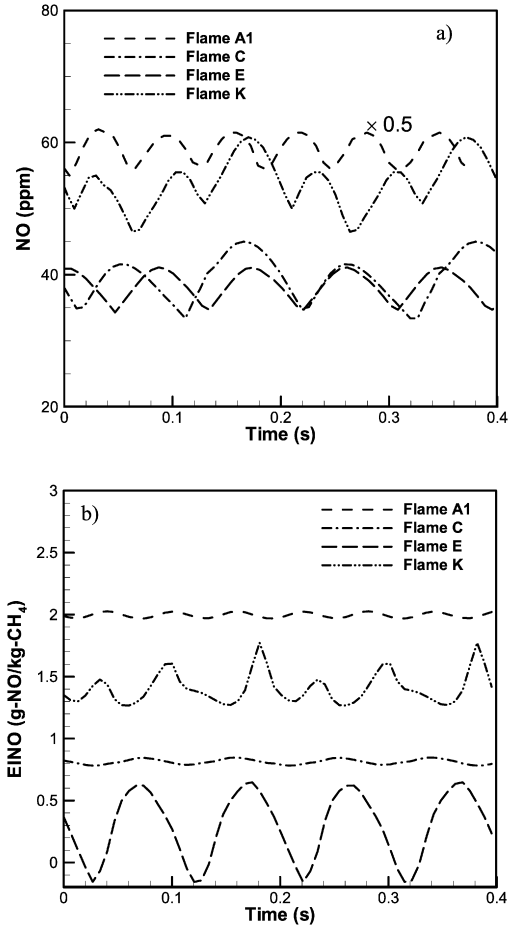

Fig. 9. Temporal evolution of the (a) maximum NO and (b) EINO for various multistage coflow flames established at $\phi_R = \phi_L = 1.0$ (Flame A1), $\phi_R = 1.5$ and $\phi_L = 0.8$ (Flame C), $\phi_R = 2.0$ and $\phi_L = 0.6$ (Flame E), and $\phi_R = 3.5$ and $\phi_L = 0.0$ (Flame K).

Fig. 9 indicates that mean values of NO mole fraction and EINO first decrease and then increase going from the premixed flame regime (Flame A1) to the triple flame regime (Flames C and E) and then to the double flame regime (Flame K). This behavior is again similar to that observed for counterflow flames.

Fig. 10 presents the time-averaged EINO plotted as a function of ϕ_R and ϕ_L for various coflow flames established at a global $\phi = 1.0$. The time-averaged EINO in axisymmetric configuration is defined as

$$\mathrm{EINO} = \frac{1}{\tau}\int_0^{\tau} \frac{1000\int_0^{Lz}\int_0^{Lr} \mathrm{MW_{NO}}\omega_{\mathrm{NO}} r\,\mathrm{d}r\,\mathrm{d}z}{-\int_0^{Lz}\int_0^{Lr} \mathrm{MW_{CH_4}}\omega_{\mathrm{CH_4}} r\,\mathrm{d}r\,\mathrm{d}z}\,\mathrm{d}t \quad (\mathrm{g\ NO/kg\ CH_4}), \tag{6}$$

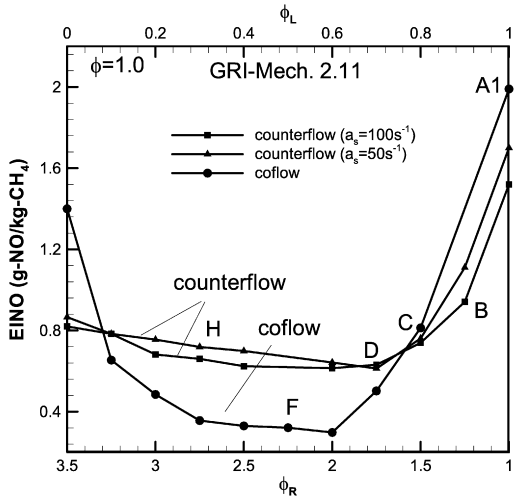

Fig. 10. Comparison of the NO emission index (EINO) of counterflow and coflow flames as a function of ϕ_R for a global $\phi = 1.0$. For coflow flames, the EINO values are time-averaged.

where τ is the time period. The results for the corresponding counterflow flames established at global $\phi = 1.0$ and two different strain rates, $a_S = 50$ and 100 s^{-1}, are also presented for comparison. An important result from this figure is that despite the difference in geometry, the counterflow and coflow flames exhibit qualitatively similar NO_x characteristics with regard to the effect of partial premixing. At a fixed global ϕ, there is an optimum level of partial premixing that yields the lowest NO_x emission in both configurations. There are of course quantitative differences in NO_x emissions in the two configurations, which can be attributed to geometry-dependent effects. For instance, in the triple flame regime (Flames D through J), the coflow flames have a lower NO_x emission index than the counterflow flames, which may be attributed to the fact that the coflow flames have much larger flame volume and, therefore, lower peak flame temperatures than those in counterflow flames. As mentioned earlier, going from Flame A1 to Flame K, the flame length and volume increase in coflow flames, while they decrease in counterflow flames. Moreover, the amount of fuel consumed in counterflow flames is significantly smaller than that in coflow flames, as counterflow flames are known to be highly inefficient in terms of fuel consumption, and this could lead to a higher emission index for these flames. Other geometry-dependent differences include (i) the buoyancy-induced oscillations and (ii) heat losses to the burner rim in the case of coflow flames, although the latter effect is not expected to be significant since the amount of NO_x formed near the burner rim is negligible [23].

4. Conclusions

We have simulated both coflow and counterflow methane–air flames over a complete partially premixed regime and characterized the effects of dominant combustion modes (i.e., single-, two-, and three-stage combustion) on NO_x emissions. Simulations employ a comprehensive numerical model that uses a detailed description of transport and flame and NO_x chemistries (GRI-2.11) and includes radiation effects.

1. It has been demonstrated that a complete partially premixed regime, which extends from premixed flames to triple flames and then to double flames, can be simulated in both the coflow and counterflow configurations by suitably varying the rich (ϕ_R) and lean (ϕ_L) equivalence ratios, while maintaining the global equivalence ratio (ϕ) fixed. This allows us to characterize NO_x emissions in the entire partially premixed regime, as the global flame structure transitions from a premixed flame to a triple flame containing three reaction zones, and then to a double flame containing two reaction zones.
2. Both counterflow and coflow flame simulations show that at a fixed global ϕ, as ϕ_R is increased with corresponding decrease in ϕ_L, the NO_x concentration and emission index ($EINO_x$) first decrease from the premixed to the triple flame regime, and then increase from the triple to the double flame regime. This is a significant result, since for the first time, the entire partially premixed regime has been simulated, and the existence of an optimum level of partial premixing (in terms of ϕ_R and ϕ_L) for the lowest NO_x emission has been demonstrated. In addition, it has been shown that triple flames not only extend the rich and lean flammability limits, but also exhibit superior NO_x characteristics compared to the corresponding premixed and partially premixed (double) flames.
3. Contributions of the various submechanisms to total NO_x have been quantified in the entire partially premixed regime. The thermal and prompt NO are the dominant contributors to total NO_x, while NNH-intermediate and N_2O-intermediate routes make small but nonnegligible contributions. The contribution of NO_2 is negligible for the conditions investigated. In addition, at a fixed global ϕ, as ϕ_R is increased with corresponding decrease in ϕ_L, the contribution of thermal NO progressively decreases while that of prompt NO increases. This explains the nonmonotonic variation of $EINO_x$ with the level of partial premixing.
4. Coflow and counterflow flames exhibit qualitatively similar NO_x characteristics in the entire partially premixed regime. There are, however, quantitative differences that can be attributed to geometry-dependent effects. For example, coflow flames have significantly larger flame volume and therefore lower peak temperature and lower NO_x compared to the counterflow flames in the triple flame regime.

References

[1] H. Phillips, Proc. Combust. Inst. 10 (1965) 1277–1283.
[2] J. Buckmaster, M. Matalon, Proc. Combust. Inst. 22 (1988) 1527–1535.
[3] J.W. Dold, Combust. Flame 76 (1989) 71–88.
[4] L.J. Hartley, J.W. Dold, Combust. Sci. Technol. 80 (1991) 23–46.
[5] P.N. Kioni, B. Rogg, K.N.C. Bray, A. Liñán, Combust. Flame 95 (1993) 276–290.
[6] G.R. Ruetsch, L. Vervisch, A. Liñán, Phys. Fluids 7 (6) (1995) 1447.
[7] J. Daou, A. Liñán, Combust. Theory Modelling 2 (1998) 449–477.
[8] J. Buckmaster, Y. Zhang, Combust. Theory Modelling 3 (1999) 547–565.
[9] R.W. Thatcher, J.W. Dold, Combust. Theory Modelling 4 (2000) 435–457.
[10] I.K. Puri, S.K. Aggarwal, S. Ratti, R. Azzoni, Combust. Flame 124 (2001) 311–325.
[11] H. Guo, F. Liu, G.J. Smallwood, Combust. Flame 143 (2003) 282–298.
[12] X.L. Zhu, M.N. Nishioka, T. Takeno, Proc. Combust. Inst. 27 (1998) 1369–1376.
[13] P. Domingo, L. Vervisch, Proc. Combust. Inst. 26 (1996) 233–240.
[14] B.J. Lee, S.H. Chung, Combust. Flame 109 (1997) 163–172.
[15] S. Ghosal, L. Vervisch, Combust. Flame 123 (2001) 646–655.
[16] X. Qin, I.K. Puri, S.K. Aggarwal, Proc. Combust. Inst. 29 (2002) 1565–1572.
[17] A.J. Lock, A.M. Briones, X. Qin, S.K. Aggarwal, I.K. Puri, U. Hegde, Combust. Flame 143 (2005) 159–173.
[18] N. Peters, F.A. Williams, AIAA J. 21 (1983) 423–429.
[19] W.M. Pitts, Proc. Combust. Inst. 22 (1988) 809–816.
[20] J.E. Dec, A conceptual model of DI diesel engine combustion based on a laser-sheet imaging, SAE Paper 970873, 1997.
[21] D.T. Montgomery, R.D. Reitz, Effects of multiple injections and flexible control of boost and EGR on emissions and fuel consumption of a heavy-duty diesel engine, SAE Paper 01-0195, SAE World Congress, Detroit, MI, 2001.
[22] S.K. Chen, Simultaneous reduction of NO_x and particulate emissions by using multiple injections in a small diesel engine, SAE Paper 01-3084, SAE World Congress, Detroit, MI, 2000.
[23] R. Azzoni, S. Ratti, S.K. Aggarwal, I.K. Puri, Combust. Flame 119 (1/2) (1999) 23–40.

[24] X. Qin, C. Choi, I.K. Puri, S.K. Aggarwal, Combust. Theory Modeling 8 (2) (2004) 293–314.
[25] S.C. Li, F.A. Williams, Combust. Flame 188 (1999) 399–412.
[26] H. Xue, S.K. Aggarwal, Combust. Flame 132 (2003) 723–741.
[27] J.P. Gore, N.J. Zhan, Combust. Flame 105 (1996) 414–427.
[28] M.A. Tanoff, M.D. Smooke, R.J. Osborne, T.M. Brown, R.W. Pitz, Proc. Combust. Inst. 26 (1996) 1121–1128.
[29] A.E. Lutz, R.J. Kee, J.F. Grear, F.M. Rupley, Sandia National Laboratories Report No. SAND96-8243.
[30] R.J. Kee, F.M. Rupley, J.A. Miller, Sandia National Laboratories Report No. 89-8009B.
[31] S. Som, M.S. thesis, University of Illinois at Chicago, 2005.
[32] V.R. Katta, L.P. Goss, W.M. Roquemore, Combust. Flame 96 (1994) 60.
[33] Z. Shu, S.K. Aggarwal, V.R. Katta, I.K. Puri, Combust. Flame 111 (1997) 276.
[34] C.T. Bowman, R.K. Hanson, D.F. Davidson, W.C. Gardiner Jr., V. Lissianski, G.P. Smith, D.M. Golden, M. Frenklach, M. Goldenberg, available at http://www.me.berkeley.edu/gri_mech/, Version 2.11.
[35] G.P. Smith, D.M. Golden, M. Frenklach, N.W. Moriarty, B. Eiteneer, M. Goldenberg, C.T. Bowman, R.K. Hanson, S. Song, W.C. Gardiner Jr., V.V. Lissianski, Z. Qin, GRI Mech-3.0, available at http://www.me.berkeley.edu/grimech/, 1999.
[36] G. Rozenchan, D.L. Zhu, C.K. Law, S.D. Tse, Proc. Combust. Inst. 29 (2002) 1461–1469.
[37] R. Evertsen, J.A. Van Oijen, R.T.E. Hermanns, L.P.H. De Goey, J.J. Ter Meulen, Combust. Flame 132 (2003) 34–42.
[38] R.V. Ravikrishna, N.M. Laurendeau, Combust. Flame 122 (2000) 474–482.
[39] T. Shimizu, F.A. Williams, in: 43rd AIAA Meeting, Nevada.
[40] A.M. Briones, S.K. Aggarwal, V.R. Katta, Phys. Fluids 18 (2006) 043603.
[41] Z. Shu, B. Krass, C. Choi, S.K. Aggarwal, V. Katta, I.K. Puri, Proc. Combust. Inst. 27 (1998) 625–634.
[42] R. Azzoni, S. Ratti, I.K. Puri, S.K. Aggarwal, Phys. Fluids 11 (1999) 3449–3464.
[43] J. Lim, J. Gore, R. Viskanta, Combust. Flame 121 (2000) 262–274.
[44] B.A. V Bennett, C.S. Mcenally, L.D. Pfefferle, M.D. Smooke, Combust. Flame 123 (2000) 522–546.
[45] R.S. Barlow, A.N. Karpetis, J.H. Frank, J.Y. Chen, Combust. Flame 127 (2001) 2102–2118.
[46] H.S. Xue, S.K. Aggarwal, R.J. Osborne, T.M. Brown, R.W. Pitz, AIAA J. 40 (2002) 1236–1238.
[47] L.G. Blevins, J.P. Gore, Combust. Flame 116 (1999) 546–566.
[48] C.K. Law, C.J. Sung, Prog. Energy Combust. Sci. 26 (2000) 459–505.
[49] S.R. Turns, An Introduction to Combustion: Concepts and Applications, second ed., McGraw–Hill, 2000.
[50] S. Naha, S.K. Aggarwal, Combust. Flame 139 (2004) 90–105.
[51] T. Takeno, M. Nishioka, Combust. Flame 92 (1993) 465–468.
[52] S.V. Naik, N.M. Laurendeau, Combust. Sci. Technol. 176 (2004) 1809–1853.